Exploring Dynamic P-Q Capability and Abnormal Operations of Inverter Based Resources

Himadry Shekhar Das, *Student Member, IEEE*, Shuhui Li, *Senior Member, IEEE*, Bing Lu, Jing Wang, *Senior Member, IEEE*, Shahinur Rahman, *Student Member, IEEE*, and Xingang Fu, *Member, IEEE*

***Abstract* -- Nowadays, inverter-based resources (IBRs) are growing very quickly in electric power systems. On the other side, abnormal IBR operations are also occurring more often. Traditionally, IBR PQ capability charts are employed by electric utility companies for safe and reliable operations of IBRs. However, it is found in this paper that existing IBR PQ capability charts do not capture the operating characteristics of an IBR correctly, which can result in irregular and unstable IBR operations. In this paper, a novel study about IBR PQ capability charts is presented where specific IBR constraints, such as rated power/current and PWM saturation constraints are considered. The results show that the IBR PQ capability charts exhibit a unique dynamic nature under uncertain grid conditions, which has not been considered by the industry in managing, designing, and controlling an IBR as well as developing international standards for the interconnection of IBRs in the distribution and transmission systems. Through both electromagnetic transient simulation and hardware experimental investigations, it is found in this paper that the dynamic PQ capability natures, together with the limitations of the existing control methods, are the underlying causes of many unusual IBR operations that have been reported in the literature.**

***Keywords*--inverter-based resources, PQ capability charts, grid-connected filters, subsynchronous resonance, weak grid, inverter momentary cessation**

I. Introduction

THE rapid grid integration of renewable energy sources, including solar photovoltaic (PV), wind turbines (WTs), fuel cells etc., have influenced the power grid of the United States as well as all over the world. These renewable energy resources are integrated into the power grid using power electronic converters, thus named as inverter-based resources (IBRs).

Conventionally, for a synchronous generator, PQ Capability charts are used to define the reliable operation boundary of the machine and is used to manage the generator controller [1, 2]. Similarly, the IBR PQ capability is one of the most important specifications of international IBR standards [3, 4]. Several IBR PQ capability charts have been developed. The ERCOT (Electric Reliability Council of Texas) introduced a rectangle shape PQ capability chart which requires to be satisfied at the POI (Point of Interconnection) (Fig. 1a) [5]. The reliability guideline of NERC (North America Electric Reliability Corp.) described in [6] proposed a near semi-circle PQ capability chart for nominal voltage with a fixed reactive power at about 95% of the active output power (Fig. 1b).

A. Problem descriptions

An IBR has a very sophisticated control system that differs from a synchronous generator, and its operation is highly dynamic and restricted by several constraints that are totally different from a synchronous generator, such as the saturation of pulse-width modulation (PWM). Besides, a grid-connected filter is mandatory for connecting an IBR to the grid. Nevertheless, the existing PQ capability charts developed by the IBR industry do not have adequate consideration of the constraints and characteristics specific to an IBR.

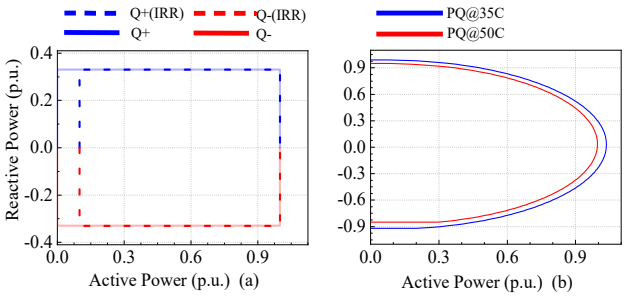

Fig. 1. Commonly used IBR PQ capability curves from (a) ERCOT [5] and (b) NERC [6]

On the other hand, many abnormal IBR operations have been reported in the literature. [7] presents field records of unstable operations from grid-tied solar plants and points out that the causes of the instabilities may involve interactions among solar inverter control systems and grid impedance characteristics. [8] demonstrates even more strange events where Type-4 WT and solar PV farms face significant generation loss during the ordinary capacitor switching operations by electric utility companies, which has caused great ambiguity among the involved parties due to the unavailability of clear industry guidelines. Moreover, various challenges in power system protection are identified and reported in [9], which points out that many power system protection issues are difficult to understand due to abnormal operations of IBRs under faults. Many recent research articles pointed out that weak grids could be the cause for a lot of abnormal and unstable operations and momentary cessations of IBRs [10-12].

H.S. Das, S. Li, B. Lu, and S. Rahman are with the Department of Electrical & Computer Engineering, The University of Alabama, Tuscaloosa, AL 35487 USA (e-mails: hdas@crimson.ua.edu, sli@eng.ua.edu, blu2@crimson.ua.edu, srahman6@crimson.ua.edu).

J. Wang is with the National Renewable Energy Laboratory, Golden, CO 80401, USA (e-mails: jing.wang@nrel.gov).

X. Fu is with the Dept. of Elec. Eng. and Computer Sci., Texas A&M University -Kingsville, Kingsville, TX 78363 USA (e-mail: xingang.fu@tamuk.edu)

B. Needs and urgency for the proposed study

At present, abnormal IBR operations are usually thought to be a cause of (1) subsynchronous oscillation (SSO) also called subsynchronous resonance (SSR), (2) momentary cessation (MC), or (3) instability in weak grid operation.

The SSO can endanger the operation of the entire bulk power systems by causing instabilities and, hence severe damage of systems' electrical equipment [13, 14]. Several SSO events were reported between 2012 to 2014 in the Guyuan wind farm of North China [15]. More than a thousand wind turbine generators were tripped during several of those SSO events [16]. [17] also evaluated the SSO phenomena with an aggregated PV system. Normally, it is thought that an SSO is caused by resonance from power systems. However, this is not convincing because the number of SSO events are increasing for IBRs particularly.

MC refers to an inverter control mode when the IBR temporarily ceases to output any current but retains the capacity to restore the IBR operation immediately when the system voltage and system frequency are restored within the specified ranges [18, 19]. Recent NERC documents based on California and Texas events [20-23] show that IBR MC can cause serve stability issues for the bulk power system (BPS). During the discussion in the 2022 IEEE PES General Meeting in Denver, the industry urgently needed to know why such events happened and how to prevent them from happening again.

A power grid with low short circuit ratio (SCR) or high line impedance is called weak grid [24]. It has been reported that in the weak grid conditions, IBRs especially are fragile and have low stability strength [24-26], which can cause the trip, MC, and SSO of IBRs. However, it was also pointed out by the industry experts from IEEE P2800 working groups [27] that in the strong grid conditions, IBR trip, MC, and SSO events still happened frequently.

We found in the study of this paper that many irregular operations of IBRs are in fact directly or indirectly related to the dynamic PQ capability nature of an IBR and limitations of existing control technologies, which has not been reported in the literature and considered by the industry in an IBR system design. As a result, it is urgently important to conduct a comprehensive IBR PQ capability study by considering IBR control characteristics, filtering mechanisms, grid voltage impact, parameter change impact, and impact of different pulse-width modulation schemes as well as whether existing IBR control technologies are affected under the dynamic PQ capability conditions.

C. Impacts of the proposed research

Based on the review and issues presented above, this paper gives novel contributions regarding the following questions that are important to the IBR industry and research community: 1) how to develop correct IBR PQ capability charts? 2) what unique characteristics do IBR PQ capability charts present? 3) can IBR PQ capability charts be employed to ensure safe IBR operation? 4) what limitations are associated with conventional IBR control methods? and 5) what the root causes are for many IBR abnormal operations reported in the literature.

To the best of our knowledge, these questions have not been investigated in details the existing literature. Therefore, the study shown in this paper would help the industry to detect the root causes of numerous irregular and unstable IBR operations mentioned in the literature and discussed above. In a nutshell, this article will assist the development of accurate industry standards and establish the research foundation to develop advanced control algorithms for IBR grid integration to overcome the challenges faced by the inverter and utility industry.

The remaining article is organized as the following. Section II presents the fundamental properties of IBR and gives the IBR power models in *dq*- reference frame. The algorithms to obtain IBR PQ capability charts are presented in Section III. A comprehensive IBR PQ capability assessment is provided in Section IV. Section V shows EMT simulation to assess the impacts of dynamic PQ capability on abnormal IBR control and operations. Section VI gives hardware experiment evaluation. Finally, the paper gives summary remarks.

II. Inverter-Based Resources, Grid Interconnection and Control

A. Inverter-based resources and control

An IBR for solar PV generator, battery storage, and Type-4 WT has a general configuration as illustrated in Fig. 2a [12-15], which is the focus of this paper. The source-side converter for PV generator and battery is a *dc-dc* converter, and for a Type-4 WT, it is an *ac-dc* converter, and the grid-side converter is a *dc-ac* inverter for all the three cases. The control action of the source-side converter is to either extract maximum power for PV and WT, or to manage charging/discharging of the battery, whereas the responsibility of the grid-side converter controller is to maintain a stable *dc*-link voltage and adjust the reactive power flow according to the grid requirement. For an IBR to the grid as a whole, it is analogous to postulate that the voltage of the *dc*-link does not change, and the grid-side inverter controller (Fig. 2b) has a cascaded outer-loop active power and reactive power controller plus an inner-loop current controller, typically designed in the *d-q* reference frame based upon the voltage orientation at the point of common coupling (PCC) with the power system. The active and reactive power controller in the outer-loop produces *d*-axis and *q*-axis current references and the current controller in the inner-loop produces *d*-axis and *q*-axis control voltage signals, $v^*_{d\_inv}$ and $v^*_{q\_inv}$. At the inverter terminal, the voltage injected to the BPS, v_{dq_inv}, is related to the controller output voltage as follows [28],

$$v_{dq\_inv} = k_{PWM} \cdot v^*_{dq\_inv} \tag{1}$$

where k_{PWM} stands for the PWM ratio between the inverter terminal voltage and the output voltage of the controller [28].

The main objective of the power control loops is to control the active and reactive power flow of the IBR to the grid at the *PCC*. The active and reactive power references P^*_{PCC} and Q^*_{PCC} are provided to the controller while the power control loops try to maintain inverter output power at the steady state to the reference values. To ensure the reliable operation of the IBR,

the reference power supplied to the controller has to be within the PQ capability limits of the IBR imposed by the physical constraints of the grid-connected inverter.

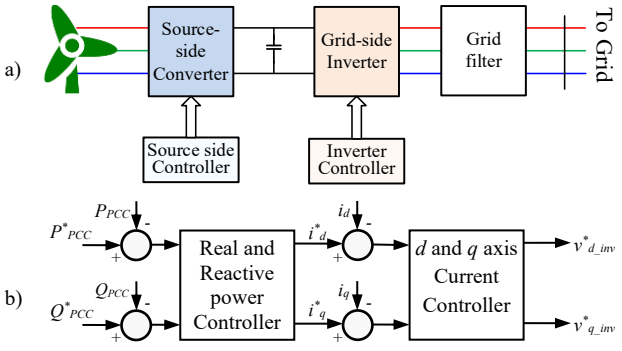

Fig. 2. Inverter based resources diagram a) IBR with converters and controllers, b) Equivalent controller for grid-side inverter

B. IBR output power at the PCC

As shown in Fig. 2b, the inverter controller design follows the *d-q* reference frame theory. Hence, to understand how the IBR *PQ* capability should be considered in building the IBR control for the IBR grid interconnection, it is important to derive the IBR steady-state output power model at the *PCC* using the *dq* reference frame.

Typically, the power output at the *PCC* depends on the inverter output voltage in the *ac* system, the grid voltage, and types and parameters of the grid connected filter. Three grid connected filters are commonly used. They are *L*, *LC* and *LCL* filters. Fig. 3 presents the schematic diagram of a grid connected inverter interfaced to the grid using an *LCL*-filter, where R_{inv} and L_{inv} represents the inverter-side inductor resistance and inductance, *C* is the filter capacitor, L_g and R_g are the inductance and resistance of the grid-side inductor.

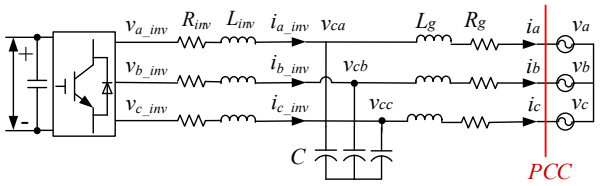

Fig. 3 Grid-connected inverter schematic based on LCL filter

By following the generator sign convention, the voltage balance equation across the inverter-side inductor is [29]

$$v_{dq\_inv} = R_{inv} \cdot i_{dq\_inv} + L_{inv} \cdot di_{dq\_inv}/dt + j\omega_s L_{inv} \cdot i_{dq\_inv} + v_{cdq}, \quad (2)$$

the voltage balance equation across the grid-side inductor is

$$v_{cdq} = R_g \cdot i_{dq} + L_g \cdot di_{dq}/dt + j\omega_s L_g \cdot i_{dq} + v_{dq}, \quad (3)$$

and the current balance equation of the filter capacitor is:

$$i_{dq\_inv} = i_{dq} + C \cdot dv_{dq}/dt + j\omega_s C \cdot v_{cdq} \quad (4)$$

where the *dq* voltage at the *PCC* is $v_{dq}=v_d+jv_q$, in which v_d and v_q are the *d* and *q* components of the *PCC* voltage; the *dq* current flowing into the grid is i_{dq}; the *dq* capacitor voltage is v_{cdq}; the *dq* inverter output voltage and current are v_{dq_inv} and i_{dq_inv}, respectively.

In the steady-state, (2) - (4) become (5) - (7) as

$$V_{dq\_inv} = R_{inv} \cdot I_{dq\_inv} + j\omega_s L_{inv} \cdot I_{dq\_inv} + V_{cdq} \quad (5)$$

$$V_{cdq} = R_g \cdot I_{dq} + j\omega_s L_g \cdot I_{dq} + V_{dq} \quad (6)$$

$$I_{dq\_inv} = I_{dq} + j\omega_s C \cdot V_{cdq} \quad (7)$$

where V_{dq_inv}, I_{dq_inv}, V_{cdq}, I_{dq} and V_{dq} represent the steady-state *d-q* vectors of inverter output voltage, inverter-side inductor current, capacitor voltage, grid-side inductor current, and *PCC* voltage. From (5) - (7), the steady state current flowing to the BPS at the *PCC* can be obtained as follows

$$I_{dq} = \frac{V_{dq\_inv} - V_{dq}\left(1 + j \cdot Z_{inv}/X_C\right)}{Z_{inv} + Z_g + j \cdot Z_{inv} Z_g / X_C} \quad (8)$$

where $Z_{inv}= R_{inv} + j\omega_s L_{inv}$ and $Z_g= R_g + j\omega_s L_g$ stand for the impedances of the inverter-side and grid-side inductors, respectively. Thus, the power supplied to the power grid from the IBR at the *PCC* can be obtained as follows

$$P_{PCC} + jQ_{PCC} = V_{dq} I^*_{dq} = V_d I^*_{dq} \quad (9)$$

where the *PCC* voltage alignment is employed.

III. Determine IBR PQ Capability Regions

The IBR *PQ* capability region represents the permissible output power region considering the physical constraints of the IBR, i.e., 1) rated power/current constraint and 2) PWM saturation constraint. The control of an IBR inverter must ensure its operation within the *PQ* capability region. In other words, the power references, P^*_{PCC} and Q^*_{PCC}, presented to the IBR controller (Fig. 2b) cannot be over the permissible *PQ* capability region for safe and reliable operation of the IBR. The algorithms to calculate IBR *PQ* capability charts are developed in the following subsections.

A. PQ capability under rated power/current constraint

Assume the IBR rated apparent power is S_{rated}. Then, at the nominal *PCC* voltage condition, the power references presented to the inverter controller, as illustrated in Fig. 2b, must satisfy the following equation:

$$\sqrt{\left(P^*_{PCC}\right)^2 + \left(Q^*_{PCC}\right)^2} \le S_{rated} \quad (10)$$

where P^*_{PCC} can either be positive (i.e., generating for wind, solar and battery discharging) or negative (i.e., absorbing for battery charging), and Q^*_{PCC} can be of both polarities.

However, if the voltage at the *PCC* is unknown and differs from the nominal voltage, the *PQ* capability calculation using (10) might not provide the correct value. For example, during a low-voltage ride-through event, the actual *PCC* voltage can fall to a much lower value than the nominal voltage, and the PQ capability calculation using (10) might provide an IBR current value which is much higher than the rated current of the IBR. Since an IBR is fragile to over current, the *PQ* capability should be obtained according to the current rating instead of the power rating as follows

$$\sqrt{\left(I^*_d\right)^2 + \left(I^*_q\right)^2} \le I_{rated} \quad (11)$$

B. PQ capability under PWM saturation constraint

Besides the rated current constraint, the output power of an IBR is also limited by the PWM saturation constraint, depending on what type of a PWM scheme is employed. Typically, there are two PWM schemes: sinusoidal PWM (SPWM) and space vector PWM (SVPWM) [18]. Overall, the *d*-axis and *q*-axis voltages at the output terminal of the inverter, v_{d_inv} and v_{q_inv}, should meet the equation below:

$$\sqrt{v_{d\_inv}^2 + v_{q\_inv}^2} \le V_{dq\_\max} \tag{12}$$

where V_{dq_max} is $\sqrt{3}V_{dc}/\left(2\sqrt{2}\right)$ for SPWM and $V_{dc}/\sqrt{2}$ for SVPWM [16, 18]. Hence, the permissible *PQ* capability region at an arbitrary *PCC* voltage under the PWM saturation constraint can be determined as follows: i) start with an IBR *dq* output voltage V_{dq_inv} whose amplitude equals to V_{dq_max}; ii) compute I_{dq} based on (8) for an IBR having an *LCL*, *LC*, or *L* filter; iii) compute the active power and reactive power transferred from the IBR to the grid at the *PCC* via (9); iv) repeat (i) to (iii) for other *dq* output voltages.

Then, an overall algorithm can be developed to compute the IBR *PQ* capability considering both constraints. Fig. 4 shows a flowchart of the algorithm. It contains three main blocks. The first block calculates the rated current *PQ* capability chart, the second block calculates the PWM saturation *PQ* capability chart, and the last block gets the resultant *PQ* capability by combining the results from the other two blocks.

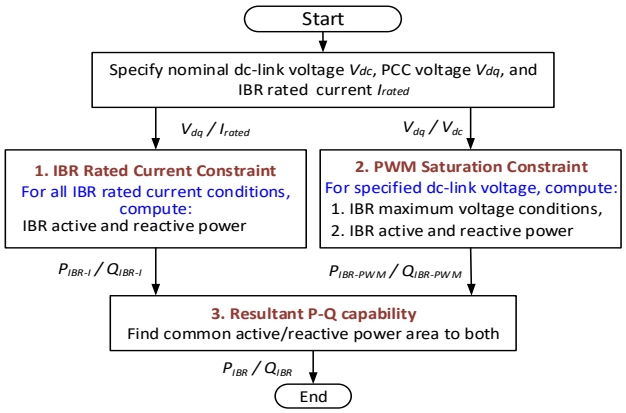

Fig. 4. A flowchart showing how to determine IBR P-Q capability charts

IV. IBR Dynamic PQ Capability Analysis

Traditionally, the *PQ* capability of an IBR is obtained at the nominal condition. However, in real-life conditions, the grid voltage is unknown, the *dc*-link voltage may change, and grid-filter parameters may be different from the nominal values, resulting in dynamic *PQ* capability characteristics for an IBR.

A. PQ capability under the nominal condition

Based on [30], the following parameters are used as the nominal values. 1) The IBR rated power is 1.5 MVA. 2) The *dc*-link voltage is 1500V. 3) The grid short-circuit MVA is about 37 MVA and the *PCC* line voltage is 60Hz, 690Vrms. 4) For the *L* filter, the inductance is 0.4mH and the inductor resistance is 0.003Ω. 5) For the *LC* filter, the inductor keeps the same, and the capacitance is 25μF. 6) For the *LCL* filter, the capacitance is the same while for both the inverter- and grid-side inductors, the inductance is 0.2mH and the inductor resistance is 0.0015Ω. Thus, the short-circuit MVA at the IBR output terminal is about 3.16MVA. All the *PQ* capability analysis in this section is in per unit (p.u.), and the base voltage and power are the nominal *PCC* voltage and IBR rated power.

At the nominal condition, the IBR maximum output voltage V_{dq_max} is 1.3312 p.u. for SPWM and 1.5372 p.u. for SVPWM. Then, the nominal *PQ* capability charts are obtained as shown in Fig. 5, in which the circle with the origin at [0, 0] signifies the rated current circle (RIC) while the others, labeled as PWMLCL, PWMLC, and PWML, are circles related to the PWM saturation constraint of the IBR with *LCL*, *LC*, and *L* filters, respectively.

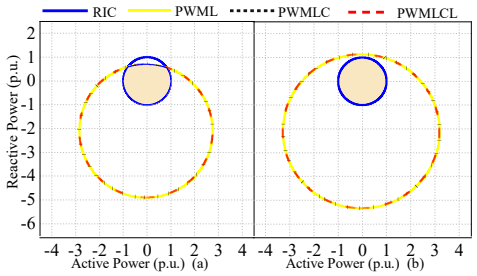

Figure 5. IBR *PQ* capability areas at the nominal condition using (a) SPWM and (b) SVPWM

As shown in Fig. 5, the PWM circles are essentially overlapped for all the three filtering schemes because the capacitor in the *LCL* and *LC* filters are primarily designed for the harmonic filtering purpose but not for the reactive power compensation. Overall, the *PQ* capability region is the joint area enclosed by the PWM saturation constraint circle and the RIC. From Fig. 5, the following remarks are acquired:

1) At the nominal condition, the *PQ* capability region is quite different from the existing IBR *PQ* capability charts utilized in the industry and from that of a synchronous generator [1,2,5,6].

2) The IBR utilizing the SVPWM shows a larger *PQ* capability region than that using the SPWM, showing that the SVPWM improves the *PQ* capability even without any added cost and size of the IBR system.

B. PQ capability at different PCC or dc-link voltages

The *PCC* and dc-link voltages have a vital impact on the PQ capability of an IBR. Fig. 6 shows a PQ capability analysis for variable *PCC* and *dc*-link voltages. Since the difference between LCL, LC, and L filters is small, only the results of the IBR with an LCL-filter are presented in the rest of this section. From Fig. 6, the following remarks are achieved:

1) If the voltage at the *dc*-link remains unchanged, the RIC expands in the PQ plane as the *PCC* voltage goes up whereas the RIC shrinks as the *PCC* voltage declines (Fig. 6b). The reason of this is that under the same nominal current, the power flowing from the IBR to the grid increases when the *PCC* voltage is higher and reduces when the *PCC* voltage is lower.

2) If the voltage at the *dc*-link is kept constant, the circle corresponding to the PWM saturation constraint expands in the PQ plane as the *PCC* voltage declines and shrinks as the *PCC* voltage increases.

3) The larger the *dc*-link voltage, the bigger the allowable PQ capability area of the IBR (Fig. 6a). Thus, a small *dc*-link voltage could restrict both active and reactive power capability of the IBR. Nevertheless, a high *dc*-link voltage would increase the cost of the IBR.

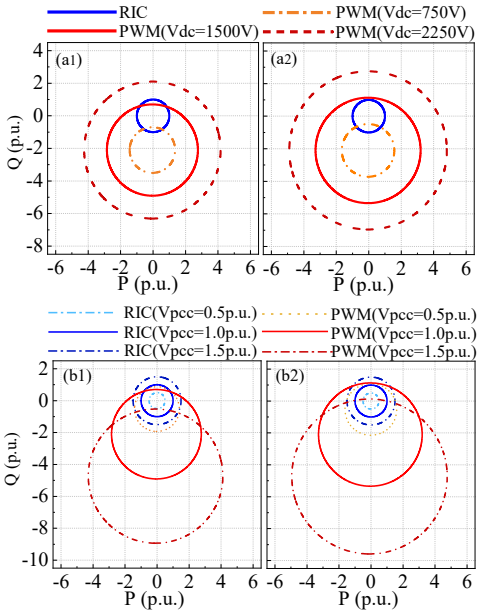

Figure 6. IBR *P*-*Q* capability charts at different *dc*-link and *PCC* voltage conditions by using SPWM (a1 & b1) and SVPWM (a2 & b2)

C. Impact of variable grid filter parameters on PQ capability

The grid-filter parameters of an IBR may be different from the nominal values specified by the factory or vary with the IBR current. The study related to variable grid-filter parameters was performed as follows: 1) retaining the filter inductance at the nominal value whereas varying the filter resistance by ±50% away from the nominal value, 2) maintaining the filter resistance at the nominal value whereas modifying the filter inductance by ±50% away from the nominal value. Fig. 7 presents the results. It was observed that the impact of the filter capacitance is very small and thus its impact is not included in the figure. The following remarks are obtained:

1) Changing the filter resistance value does not affect the *PQ* capability chart much (Fig. 7a).

2) A high filter inductance value shrinks the PWM saturation constraint circle. On the other hand, the smaller is the inductance value, the larger is the PQ capability region. But, a too small filter inductance value would decrease the harmonic restriction effect. Hence, the selection of a proper filter inductance value is a design issue that should be addressed from both the PQ capability and harmonic restriction perspectives.

V. Dynamic PQ Capability and Abnormal IBR Operation Analysis via EMT Simulation

To evaluate the *PQ* capability impact and limitations of the conventional IBR control technique, EMT simulation of a grid-connected IBR (Fig. 8) was built. It is needed to specify that under an irregular IBR operating condition, an IBR has to be tripped in order to prevent any damage so that the full process of the abnormal operation is usually unable to see or demonstrate via hardware experiments, which makes the EMT simulation significant for such an assessment.

In Fig. 8a, the grid is connected to the IBR via an RL element signifying the transmission line. The IBR consists of a PV array on the left, a *dc*-*dc* converter in the middle, and a grid-connected inverter on the right. The inverter is connected to the grid via an *LCL* filter. A small passive damping resistance is added to the *LCL* capacitor to assure the stability of the *LCL*-filter-based IBR [30]. In Fig. 8a, the MPPT controller regulates the operating point of the PV array based on the incremental conductance (IC) method to extract the maximum power from the PV array. The inverter controller controls the IBR interconnection with the grid. Fig. 8b shows the configuration of the inverter controller. The design of the inverter controllers follows the well-known standard vector control strategies [27, 28], and the following industry strategies are also built into the outer- and inner-loop controllers.

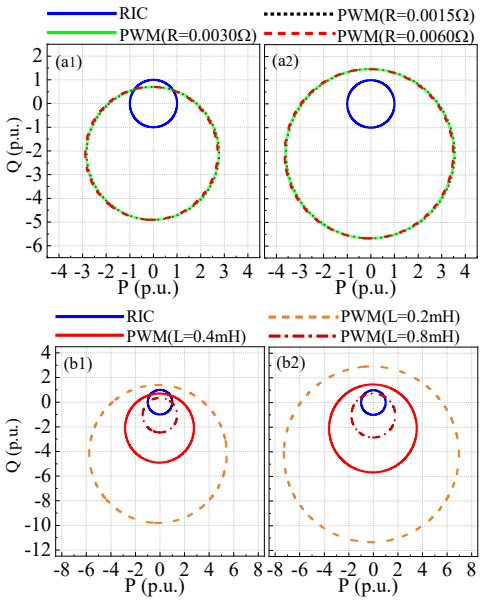

Figure 7. IBR *P*-*Q* capability areas at different IBR grid filter parameters by using SPWM (a1), (b1) and SVPWM (a2), (b2)

Firstly, for the outer-loop reactive power or *PCC* voltage controller, the reactive power reference is limited within the nominal *PQ* capability region via a reactive power limitation block utilized in the *q*-axis loop (Fig. 8b), in which Q_{max} and Q_{min} are calculated based on the reference active power command P^* and the area specified by a *PQ* capability chart such as ERCOT (Fig. 1a), NERC (Fig. 1b), etc.

Secondly, for the inner-loop current controller, a current limitation block, based upon the Active Power Priority Mode control, is utilized if $\sqrt{\left(i_d^*\right)^2+\left(i_q^*\right)^2} \ge I_{rated}$ to prevent the IBR from exceeding the rated current limit according to [3, 4]

$$i_{d\_adj}^* = i_d^*$$
$$i_{q\_adj}^* = sign\left(i_q^*\right)\sqrt{\left(I_{rated}\right)^2-\left(i_d^*\right)^2} \quad (13)$$

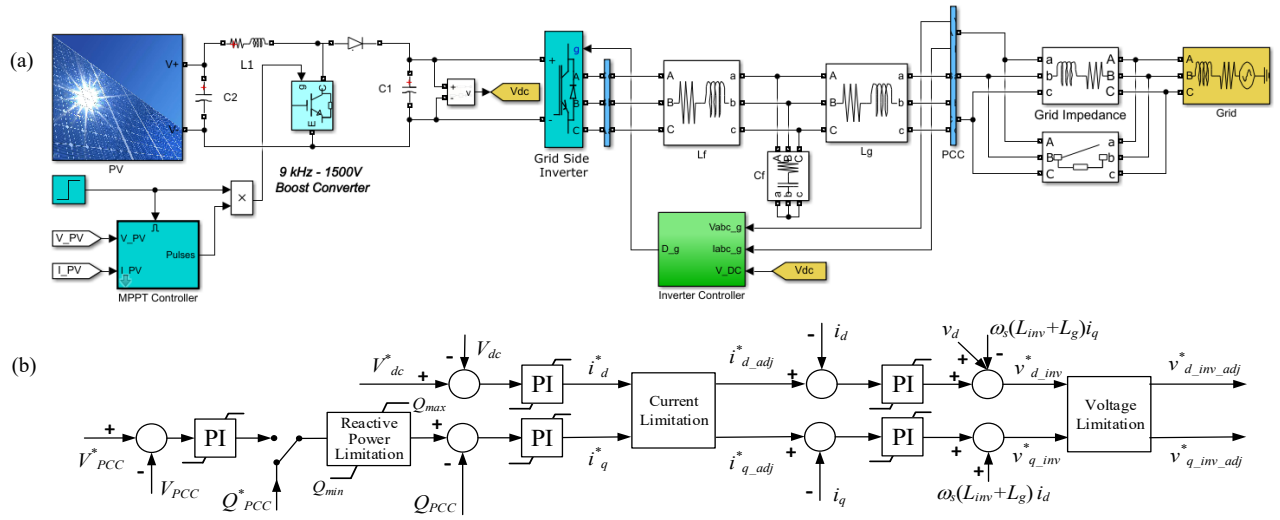

Figure 8. Illustration of EMT simulation model of a grid-connected IBR: (a) EMT simulation model in MATLAB SimPowerSystems, (b) Grid-side inverter controller structure

Thirdly, to prevent IBR from operating beyond the linear modulation limit, a voltage limitation block is utilized to the regulate the voltage generated by the current-loop controller according to [30]

$$v^*_{d\_inv\_adj} = V_{dq\_\max} \cdot \cos\left(\angle v^*_{dq\_inv}\right)$$
$$v^*_{q\_inv\_adj} = V_{dq\_\max} \cdot \sin\left(\angle v^*_{dq\_inv}\right) \quad (14)$$

Finally, a saturation mechanism is applied to all the PI controllers to prevent the integral term of a PI controller from going beyond the IBR maximum possible reactive power limit, rated current limit, and output voltage limit, respectively.

Thus, the configuration shown in Fig. 8 represents the state-of-the-art control technology used in the IBR industry.

A. PQ capability evaluation at the nominal condition

For this case, IBR grid-filter parameters and grid and *dc*-link voltages are at the nominal values. The active power is extracted from the PV array and reactive power command presented to the IBR is limited within a *PQ* capability region as follows: 1) SPWM with the nominal *PQ* capability of Fig. 5a, 2) SPWM with NERC *PQ* capability of Fig. 1b, and 3) SPWM with ERCOT *PQ* capability of Fig. 1a.

Fig. 9 presents the simulation results, in which the solar irradiation levels are specified. The extracted maximum power from the PV array as follows: 0kW at 0sec, 850kW at 0.5sec, and 400kW at 3sec. The reactive power reference is initially 400kVar and changes to 1000kVar at 1.5sec. Before 1.5sec, the extracted active power and reactive power reference (850kW and 400kVar) are within the PQ capability region for all the four cases. As shown in Fig. 9, the IBR controller can properly transfer the extracted active power to the grid, regulate the reactive power at the PCC to the reference value, and maintain the dc-link voltage at 1500V.

After 1.5sec, the extracted active power and reactive power reference (850kW and 1000kVar) are outside the PQ capability regions of Cases 1 and 3 but within the PQ capability regions of Case 2. Hence, the actual reactive power reference is adjusted from 1000kVar to 925kVar and 494kVar, respectively, according to the PQ capability regions of Fig. 5a for Case 1 and Fig. 1a for Case 3 but remains unchanged for Case 2. Thus, the reactive power after 1.5 sec is stabilized at 925kVar and 494kVar instead of 1000kVar for Cases 1 and 3, respectively. As the extracted active power drops to 400kW at 3sec, the IBR operates within the PQ capability region of Fig. 5a so that both the extracted active power and reactive power reference at the PCC are followed for Case 1, but the reactive power for Case 3 is far below the reference value showing a significant waste of the IBR capability for Case 3 (ERCOT). For Case 2 (NREC), the IBR after 1.5sec eventually gets into an oscillating state (similar to SSO) as the PQ capability is out of the actual PQ capability region shown by Fig. 5a, which would trip the IBR eventually.

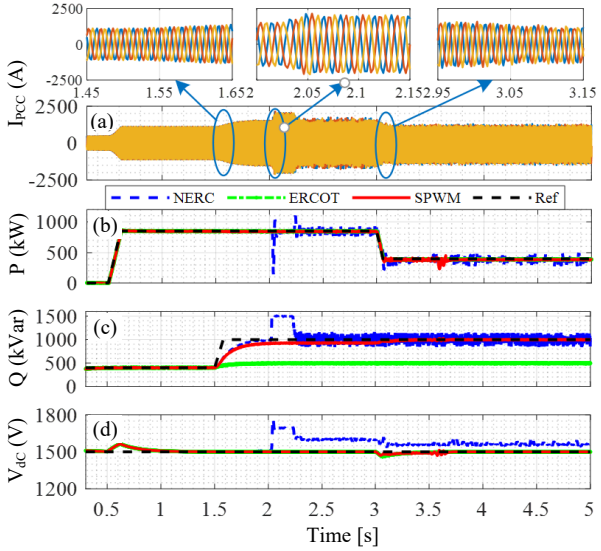

Fig. 9. EMT simulation for IBR *P-Q* capability and stability evaluation: a) *PCC* current for NERC PQ capability b) *PCC* active power, c) *PCC* reactive power, d) *dc*-link voltage

B. PQ capability evaluation as grid voltage changes

The IEEE 1547 requires that an IBR should have an adequate high and low voltage ride through capability. The impact of the *PCC* voltage is evaluated for an increase and decrease of the *PCC* voltage. Both can cause an abnormal operation of the IBR. Fig. 10 shows a case study for an increase of the *PCC* voltage

from 1 p.u. to 1.1 p.u. between 2.5 sec and 3.5 sec, in which the grid short-circuit MVA is the same as that used in Fig. 9 and the SPWM nominal PQ capability of Fig. 5a is used. The extracted PV power is initially 0kW and changes to 850kW at 0.5sec and the reference reactive power is 0kVar and changes to 800kVar at 1.5sec. The figure shows that the IBR with the SPWM becomes unable when the PCC voltage increases at 2.5sec, which could result in an MC of the IBR. This result is consistent with the PQ capability analysis shown in Fig. 5, which demonstrates the importance to consider the dynamic PQ capability nature in the IBR control design.

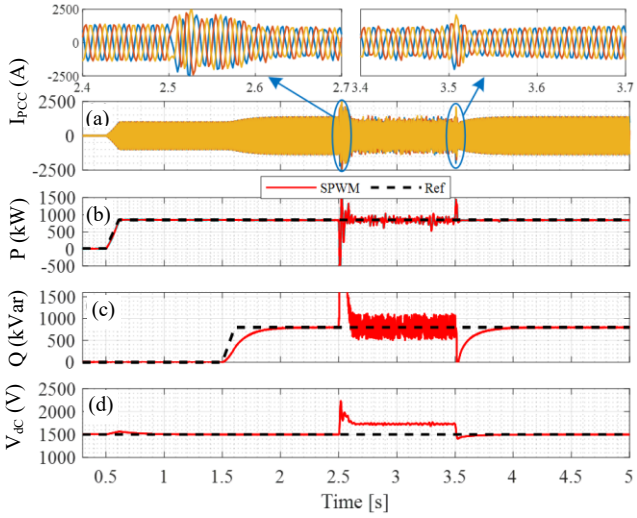

Fig. 10. *PCC* voltage impact on IBR *P-Q* capability and operation: a) PCC current for SPWM pq capability b) active power to the grid at the *PCC*, c) reactive power at the *PCC,* d) *dc*-link voltage

C. Weak grid impact and low voltage ride-through

The weak grid impact may become significant when an IBR is located at the end of a distribution feeder. The IEEE 1547 requires that an IBR should maintain the stability of its *PCC* voltage. Figs. 11 and 12 shows a case study of the IBR voltage control under a low-voltage ride-through condition caused by a fault. The extracted PV power is 400kW at 0.5sec, changes to 800kW at 5sec, and then drops to 500kW at 7sec. A fault appears between 3.5 sec and 8 sec. The grid resistance and inductance are 0.014Ω and 0.167mH, meaning that the grid short-circuit MVA at the *PCC* is about 4.68MVA. In the voltage control mode, the actual IBR PQ capability shows a more dynamic nature and is hard to determine.

For the IBR control under the four PQ capability cases, all of them start to increase the reactive power production after the fault and try to maintain the *PCC* voltage at 1 p.u. For Cases 1 and 2 (SPWM and NERC), abnormal SSO phenomena occurs shortly after the fault is started at 3.5sec. For Case 3 (ECORT), the upper limit of reactive power is reached before the IBR gets into an SSO operation, which, however, limits the maximum potential to boost the PCC voltage to 1 p.u.

D. Lesson learned from the case studies

As it is known, the *PQ* capability is a strategy that is applied to the external power control loop to assure the safe and reliable operation of an IBR. However, the studies of this paper show that the actual *PQ* capability region is highly dynamic, can be affected by many factors, and is difficult to determine in real-life conditions. As a result, one must use a static, nominal *PQ* capability chart as shown in Fig. 8b, in cooperation with two extra mechanisms, to ensure the reliable and safe operation of an IBR. One of the mechanisms is to prevent an IBR from exceeding its rated current constraint if the *PQ* capability protection applied at the external power control loop fails. The current limitation strategy (13) can effectively limit the inner current-loop controller to regulate the IBR current within its rated current region. The other is to prevent the control voltage amplitude produced by the current-loop controller from exceeding the inverter PWM saturation limit via (14). Nevertheless, (14) does not follow the common closed-loop control principle, which would make an IBR lose its controllability when such a condition arises as presented in Figs. 9 to 11.

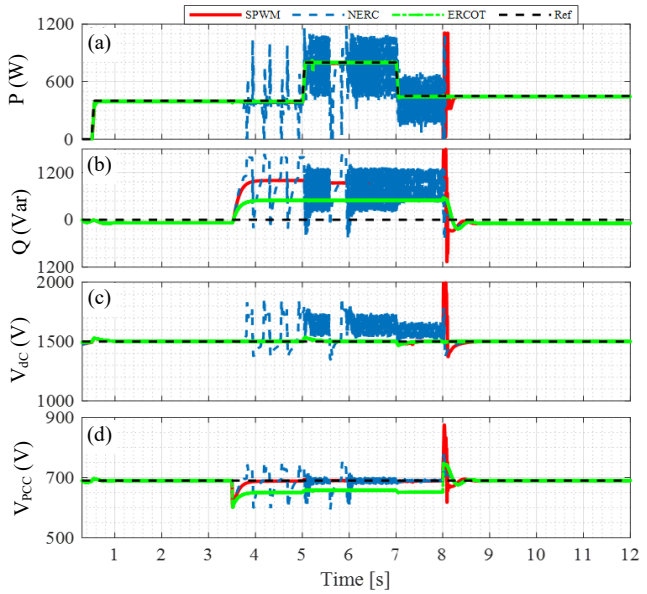

Fig. 11. IBR operation under a faulted condition: a) active power to the grid at the *PCC*, b) reactive power to the grid at the *PCC,* c) *dc*-link voltage, d) *PCC* bus voltage (RMS).

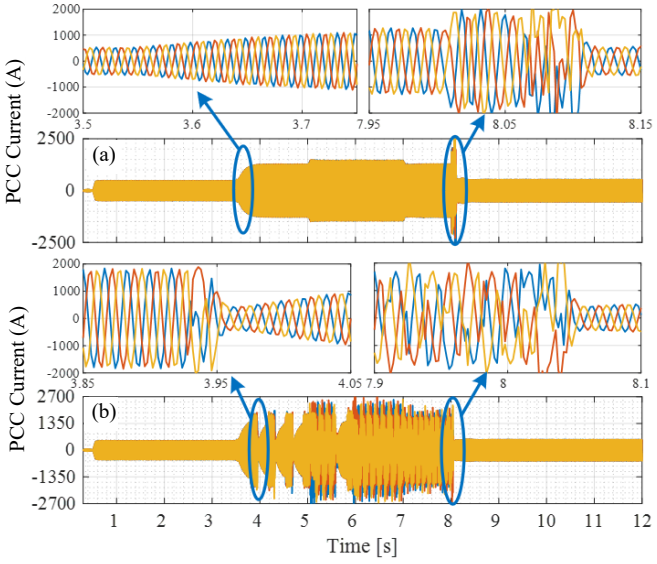

Fig. 12. IBR operation under a faulted condition: current response for a) SPWM PQ capability b) NERC PQ capability.

Overall, the study of this paper demonstrates that a fixed and nominal *PQ* capability chart, together with the existing control methods, cannot assure the reliable and safe operation of an IBR. Traditionally, when an abnormal IBR operation appeared, SSO or weak grid of the power system was typically thought to be the cause of the irregular operation. However, the study of this paper shows that unreliable IBR operations are in fact the result of the dynamic *PQ* capability nature of an IBR and the limitations of the existing control methods. Thus, to overcome the challenge, it is urgently needed to develop new IBR control technologies.

VI. Hardware Experiment

A. Experiment Setup

To further verify the case studies shown in Section V, an experiment IBR system of Fig. 8 with an LCL filter is built, as shown in Fig. 13. The experimental setup consists of four major parts: (i) a programmable *dc* power supply to represent a solar PV system, (ii) a *dc-dc* boost converter built by using a LabVolt 8857-10 IGBT converter module, (iii) a *dc-ac* inverter built by using another LabVolt 8857-10 module, (iv) a LabVolt single phase 8326-00 *LC* filter module applied with the *dc-dc* boost converter, (v) a LabVolt 3-phase 8326-00 *LCL* filter module as the grid-connected filter of the *dc-ac* inverter, (vi) two dSPACE DS1103 real-time controllers for controlling the *dc-dc* boost converter and the *dc-ac* inverter, respectively, and (vii) an OP8660 data acquisition system to get measured voltage and current signals for the DS1103 real-time controllers. The IBR is connected to the grid via a three-phase transformer. The line voltage at the *PCC* is 120V rms. The programmable DC power supply output voltage is 200V and the desired *dc* bus voltage is 240V. A load is connected at the *PCC*.

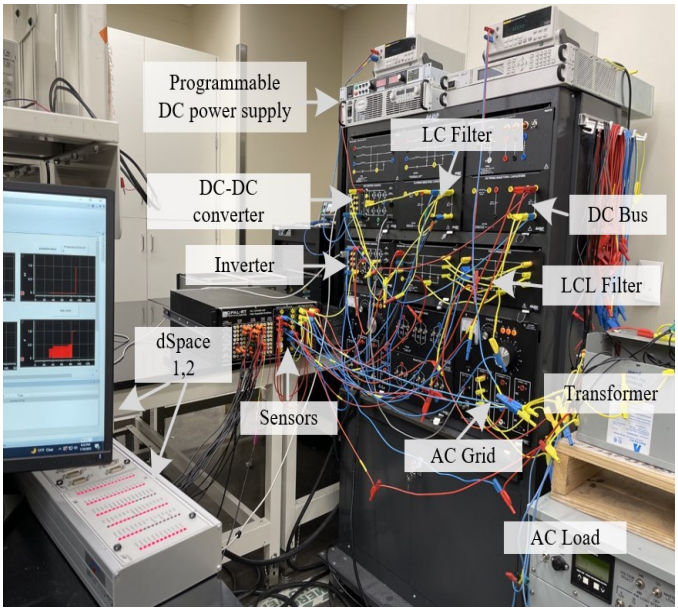

Fig. 13. Experiment setup

B. Experiment Evaluation

Figs. 14 and 15 show the experiment results for a study that is similar to the case explained in Section V.B. The IBR was set for active and reactive power control mode, in which the active power is controlled using the power tracking from the *dc* power supply, and the *dc*-bus voltage and reactive power is controlled using the cascaded control configuration as shown in Fig. 8b. The outer control loops generate d and q axis current references for the inner loop current controllers. The active and reactive power references (P^*_{PCC} and Q^*_{PCC}) were set to be within the nominal *PQ* capability region as shown in Fig. 5a. The test sequence is scheduled as follows. Initially, the load bank was connected at the *PCC* while the inverter was turned off. At t=10sec, the inverter was turned on with P^*_{PCC}=360W and Q^*_{PCC} = 0Var. As shown in Fig. 14, the IBR operated in linear modulation region (Fig. 14e) and was able to track the reference powers (Figs. 14b and 14c). At t=20sec, P^*_{PCC}=720W and Q^*_{PCC}=0Var, which was still operating within the linear modulation region. Later, Q^*_{PCC} changed to 120Var at t=34sec and 240Var at t=44sec. As shown in Fig. 14, the inverter started operating at its PWM saturation boundary after t=44sec. Although the inverter still tried to track the reference powers (Figs. 14c and 14d), the current harmonic distortion was higher as shown in Fig. 15(a).

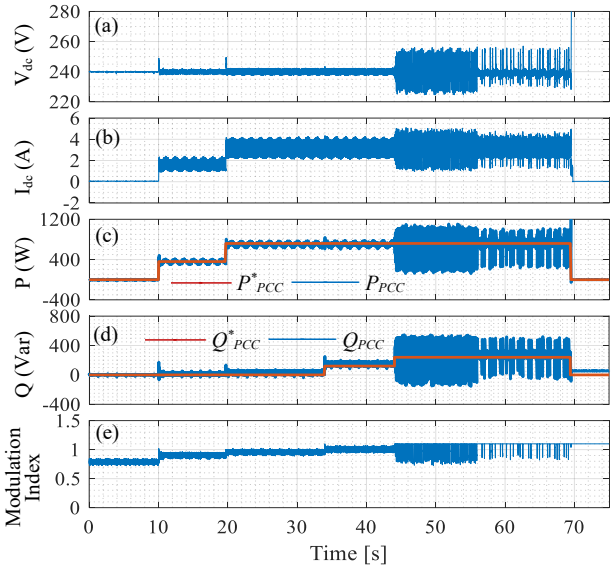

Fig. 14. Experiment results: a) DC bus voltage, b) DC bus current, c) PCC real and reactive power, d) inverter modulation index

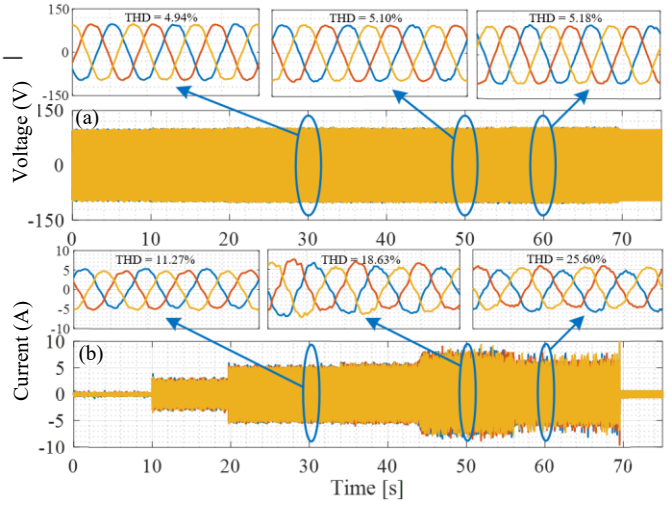

Fig. 14. Experiment results: a) PCC three phase Current, and b) PCC three phase voltage

At t=58sec, a load drop was introduced, causing the *PCC* voltage to go up and the inverter operating over the PWM saturation boundary (Fig. 14d). At t=70sec when the reactive power reference was changed to 0 VAR, the inverter was unable to track the references anymore, and there was a high current overshoot that pushed the inverter into the MC mode (Fig. 15a. The experiment evaluation is consistent with the EMT simulation study shown in Section V.

VII. Conclusions

IBR PQ capability is a critical factor for the electric power and power electronics industry to ensure the operational safety of an IBR. On the other hand, abnormal IBR operations have been increasingly reported by the power and power electronics industry. These abnormal operations were typically thought to be the cause of SSO or weak grid issues of electric power systems. The study of this article shows that practical IBR PQ capability charts are very different from the existing IBR PQ capability charts used by the industry and from those of a conventional synchronous generator and are highly dynamic under uncertain conditions of the grid, which influences the reliable and safe operation of IBRs. The study demonstrates that the dynamic nature of IBR PQ capability could cause an abnormal IBR operation under both strong and weak grid conditions and affect IBR's capability for high and low voltage ride-through. The study also identifies that when an IBR abnormal operation appears, the existing current and voltage limitation strategies applied to the conventional control methods are unable to prevent the development and expansion of the abnormal operation. The paper points out that those issues are in fact the root cause of many abnormal IBR operations reported in the literature. As a result, it is urgently needed to develop new IBR control technology to guarantee efficient and reliable IBR operation at various grid conditions.

References

[1] N.E. Nilsson and J. Mercurio, "Synchronous generator capability curve testing and evaluation," in IEEE Trans. Power Del., vol. 9, no. 1, pp. 414-424, Jan. 1994.

[2] M.M. Adibi and D.P. Milanicz, "Reactive capability limitation of synchronous machines," in IEEE Trans. Power Syst., vol. 9, no. 1, pp.29-40, Feb. 1994.

[3] IEEE Standard for Interconnection and Interoperability of Distributed Energy Resources with Associated Electric Power Systems Interfaces," in IEEE Std 1547-2018 (Revision of IEEE Std 1547-2003), vol., no., pp. 1-138, 6 April 2018.

[4] IEEE Std P2800 - Standard for Interconnection and Interoperability of Inverter-Based Resources Interconnecting with Associated Transmission Electric Power Systems, Project Details available at https://standards.ieee.org/project/2800.html.

[5] North American Electric Reliability Corporation (NERC), "Reliability Guideline BPS-Connected Inverter-Based Resource Performance," Sep. 2018, available at https://www.nerc.com/comm/OC_Reliability_ Guidelines_DL/Inverter-Based_Resource_Performance_Guideline.pdf.

[6] Electric Reliability Council of Texas (ERCOT), "Inverter-Based Resource (IBR) Workshop," available at http://ercot.com/content/wcm/key_documents_lists/176763/ERCOT_IBR_Workshop_April_25_2019.pdf.

[7] C. Li, "Unstable Operation of Photovoltaic Inverter From Field Experiences," *IEEE Trans. Power Del*, 33, no. 2, pp. 1013-1015, 2018.

[8] C. Li, "On Capacitor Switching Transient Immunity of Inverter-Based Renewable Generations," in IEEE Trans. Power Del, vol. 30, no. 5, pp. 2339-2345, Oct. 2015.

[9] IEEE Technical Report on Impact of Inverter Based Resources on Utility Transmission System Protection, prepared by Power System Relay and Control Committee Subcommittee C – System Protection Working Group C32, Jan. 2019.

[10] A. Adib, B. Mirafzal, X. Wang and F. Blaabjerg, "On Stability of Voltage Source Inverters in Weak Grids," *IEEE Access*, vol. 6, pp. 4427-4439, 2018.

[11] J. Xu, S. Xie, and T. Tang, "Evaluations of current control in weak grid case for grid-connected LCL-filtered inverter," in IET Power Electronics, vol. 6, no. 2, pp.227-234, Feb. 2013.

[12] X. Chen, Y. Zhang, S. Wang, J. Chen, and C. Gong, "Impedance-phased dynamic control method for grid-connected inverters in a weak grid," in IEEE Trans. Power Electron., 32(1), pp.274-283, 2017.

[13] North American Electric Reliability Corporation (NERC), "Reliability Considerations from the Integration of Smart Grid," Dec. 2010, available at https://www.nerc.com/files/SGTF_Report_Final_posted_v1.1.pdf.

[14] R. N. Damas, Y. Son, M. Yoon, S. -Y. Kim and S. Choi, "Subsynchronous Oscillation and Advanced Analysis: A Review," in IEEE Access, vol. 8, pp. 224020-224032, 2020, doi: 10.1109/ACCESS.2020.3044634.

[15] X. Dong, T. Xu, and Y. Zhang. "Practical SSR Incidence and Influencing Factor Analysis of DFIG-based Series-compensated Transmission System in Guyuan Farms," High Voltage Eng., vol. 43, pp. 321-328, 2017, DOI:10.13336/j.1003-6520.hve.20161227042.

[16] J. Shair, X. Xie, and L. Wang, "Overview of emerging SSO in practical wind power systems." Renewable and Sustainable Energy Reviews, vol. 99, pp. 159-168, 2019, DOI: 10.1016/j.rser.2018.09.047.

[17] R. Mahmud, A. Hoke and J. White, "Impact of Aggregated PV on Subsynchronous Torsional Interaction," 2020 47th IEEE Photovoltaic Specialists Conference (PVSC), 2020, pp. 0342-0347, doi: 10.1109/PVSC45281.2020.9300919.

[18] B. J. Pierre, M. E. Elkhatib and A. Hoke, "Photovoltaic Inverter Momentary Cessation: Recovery Process is Key," 2019 IEEE 46th Photovoltaic Specialists Conference (PVSC), 2019, pp. 1561-1565, doi: 10.1109/PVSC40753.2019.8981154.

[19] H. Shin, J. Jung, S. Oh, K. Hur, K. Iba and B. Lee, "Evaluating the Influence of Momentary Cessation Mode in Inverter-Based Distributed Generators on Power System Transient Stability," in IEEE Transactions on Power Systems, vol. 35, no. 2, pp. 1618-1626, March 2020, doi: 10.1109/TPWRS.2019.2942349.

[20] North American Electric Reliability Corporation, "Reliability Guideline: BPS-Connected Inverter-Based Resource Performance," NERC, Atlanta, GA, Sep. 2018

[21] North American Electric Reliability Corporation, "900 MW Fault Induced Solar Photovoltaic Resource Interruption Disturbance Report: Southern California Event: October 9, 2017 Joint NERC and WECC Staff Report," NERC, Atlanta, GA, Feb. 2018.

[22] North American Electric Reliability Corporation, "1,200 MW Fault Induced Solar Photovoltaic Resource Interruption Disturbance Report: Southern California 8/16/2016 Event," NERC, Atlanta, GA, June 2017.

[23] S. Zhu, D. Piper, D. Ramasubramanian, R. Quint, A. Isaacs, R. Bauer, "Modeling Inverter-Based Resources in Stability Studies," Proc. IEEE Power & Energy Society General Meeting, 2018.

[24] X. Wang, K. Qin, X. Ruan, D. Pan, Y. He and F. Liu, "A Robust Grid-Voltage Feedforward Scheme to Improve Adaptability of Grid-Connected Inverter to Weak Grid Condition," in IEEE Transactions on Power Electronics, vol. 36, no. 2, pp. 2384-2395, Feb. 2021, doi: 10.1109/TPEL.2020.3008218.

[25] X. Chen, Y. Zhang, S. Wang, J. Chen and C. Gong, "Impedance-Phased Dynamic Control Method for Grid-Connected Inverters in a Weak Grid," in IEEE Transactions on Power Electronics, vol. 32, no. 1, pp. 274-283, Jan. 2017, doi: 10.1109/TPEL.2016.2533563.

[26] D. Yang, X. Ruan and H. Wu, "Impedance Shaping of the Grid-Connected Inverter with LCL Filter to Improve Its Adaptability to the Weak Grid Condition," in IEEE Transactions on Power Electronics, vol. 29, no. 11, pp. 5795-5805, Nov. 2014, doi: 10.1109/TPEL.2014.2300235.

[27] IEEE, "IEEE 2800-2022: IEEE Standard for Interconnection and Interoperability of Inverter-Based Resources (IBRs) Interconnecting with Associated Transmission Electric Power Systems," in IEEE Std, ed: IEEE, 2022, p. 170.

[28] N. Mohan, Advanced Electric Drives, John Wiley & Sons, ISBN 978-1-118-48548-4, 2014.

[29] S. Li, T. Haskew, and L. Xu, "Conventional and Novel Control Designs for Direct Driven PMSG Wind Turbines," in Electric Power System Research, vol. 80, no. 3, pp. 328-338, March 2010.

[30] R. Gagnon and J. Brochu, "Wind Farm-Synchronous Generator and Full Scale Converter (Type 4) Detailed Model," The MathWork, Jan. 2019.
[31] R. Peña-Alzola et al., “Analysis of the passive damping losses in LCL filter-based grid converters,” in IEEE Trans. Power Electron., vol. 28, no. 6, pp. 2642–2646, Jun. 2013.